IEEE Access
Multidisciplinary ⋮ Rapid Review ⋮ Open Access Journal

Received November 3, 2020, accepted November 16, 2020, date of publication November 18, 2020,
date of current version December 9, 2020.

Digital Object Identifier 10.1109/ACCESS.2020.3039053

Decoupling Control of Permanent Magnet Synchronous Motor With Support Vector Regression Inverse System Method

MINGHUA XIE[1,2] AND LILI XIE[1], (Member, IEEE)
[1]School of Automatic, Northwestern Polytechnical University, Xi'an 710072, China
[2]School of Electronic Information and Electrical Engineering, Changsha University, Changsha 410022, China

Corresponding author: Lili Xie (xielili@nwpu.edu.cn)

This work was supported in part by the Scientific Research Fund of Hunan Provincial Education Department under Grants 20B057 and 19C0160, and in part by the National Natural Science Foundation of China under Grant 61903049.

ABSTRACT Inverse system method is effective for controlling permanent magnet synchronous motor (PMSM). A novel support vector regression(SVR) inverse system method is proposed to realize decoupling control of PMSM in the article. Firstly, kernel space feature of the inverse model is optimized by using the prior information provided by the mathematical model of analytical inverse system to build two accurate SVR inverse models, which can solve the unreasonable kernel space feature when conventional SVR algorithm is employed to model PMSM inverse system. Then, the inverse system composing of two inverse models is cascaded with the original system to decouple PMSM system into two pseudo-linear subsystems. Finally, PID controller is employed to form a closed-loop control system. The simulation and experiment results show that the proposed method improves the generalization ability of inverse model and achieves high-performance control of PMSM.

INDEX TERMS Inverse system, permanent magnet synchronous motor, support vector regression.

I. INTRODUCTION

Permanent magnet synchronous motor (PMSM) has been widely used in electric vehicles, robots, compressors and other automation equipments because of its high power density, high efficiency, simple structure and good reliability [1]–[3]. PMSM, a strong nonlinear system, is multi-variable and strongly coupled. Additionally, its parameters are variable and its load disturbances are unavoidable. Thus, it is very difficult for classical decoupling control schemes such as field-oriented control (FOC) and direct torque control (DTC) to realize high-performance control of PMSM [4]–[6].

Inverse system, an inversion of the controlled original system, is an effective method for the linearization and decoupling control of nonlinear systems [7]. Cascading the inversion with the original system, the nonlinear and coupled system is decoupled into a pseudo-linear system, which is controlled by linear control strategy. The application of inverse system requires two preconditions: one is that the original system can be represented by an accurate or approximate mathematical model, and the other is that it can be proved to be reversible.

PMSM is a complex nonlinear system. However, if some unimportant factors are ignored, an approximate mathematical model can represent it and the original system based on the model is reversible. There are two main methods for PMSM inverse system modeling: one is the analytical inverse method [8], [9], and the other is based on machine learning algorithms (MLAs) [7], [10]–[12].

Analytical inverse system model, a mathematical model based on inverse system theory and derived from the original PMSM system, cascades the original system to build a new pseudo-linear system, which is a fast way to set up a composite system. However, the mathematical model of PMSM is an ideal model with some unimportant factors such as the hysteresis in the iron core, eddy current and core magnetic saturation ignored. Moreover, stator inductance, resistance and other parameters are considered to be accurately measured and stable in any different operation condition. Therefore, the mathematical model can not fully

The associate editor coordinating the review of this manuscript and approving it for publication was Zhuang Xu.

This work is licensed under a Creative Commons Attribution 4.0 License. For more information, see https://creativecommons.org/licenses/by/4.0/

represent the actual motor and the analytical inverse model derived from it is also inaccurate.

The inverse system based on MLAs uses intelligent algorithms to build the inverse model. The training data including the factors such as hysteresis in the iron core, eddy current and core magnetic saturation ignored used in the process comes from the sampling of the original PMSM system, which is regarded as a black-box. Therefore, the dependence on the accurate mathematical model of PMSM is overcome. Liu *et al.* [10] used (Support Vector Machine)SVM to replace Neural Network to construct a PMSM inverse system and trained the SVM inverse model offline. The input features of SVM models were all normalized in order to avoid the dimension disaster. He and Wang *et al.* [11] developed an online LS-SVM (modified algorithm of the standard SVM) to construct an inverse model for pseudo-linear system. In literature [12], the BP neural network was employed to obtain the inversion of the bearingless PMSM system.

The inverse system based on MLAs overcomes the defect of analytical inverse system.However, it sets a higher demand for the inverse models. An extended closed-loop controller can be added to ensure the motor's normal operation although PMSM mathematical model of the analytical inverse system is not quite accurate, while the inverse model based on MLAs will probably affect its normal operation because of under-fitting and over-fitting that are caused by unreasonable training process of the model. Therefore, the generalization ability of inverse model is the key to the success of inverse system method.

SVR, an effective kernel-based algorithm for modeling nonlinear system [13]–[15], can balance the fitting ability of training sample data and the generalization ability of inverse models. Compared with the empirical risk minimization methods such as artificial neural network and least squares algorithm, SVR modeling based on the principle of structural risk minimization is not constrained by sample quantity and quality, thus avoiding local minimization [16]–[18].

This article proposes a SVR inverse system method for PMSM control based on kernel space feature. Firstly, the influence of input features of inverse model on the kernel space feature is analyzed and the values of feature weights are given according to the mathematical model of the original PMSM system. Then, two SVR inverse models are built to compose an inverse system. Finally, a new pseudo-linear system built by cascading the inverse system and the original system is combined with two extended PID controllers to realize high-performance closed-loop control.

The contribution of this article mainly includes two aspects. Firstly, as a PMSM inverse model is built by adopting SVR algorithm, a reasonable kernel space is constructed and the generalization ability of PMSM inverse model is also improved. Secondly, two PMSM inverse system methods based on mathematical model and on MLAs respectively are combined. The mathematical model of analytical inverse system provides important information for SVR modeling, which makes the feature of target kernel space clearer. It is of positive significance to use the model's prior information in SVR modeling for the transformation of kernel function and the construction of kernel space.

This article is organized as follows: In Section 2 ''Preliminaries'', analytical inverse system of PMSM and modeling of nonlinear system using SVR are briefly described. In Section 3 ''Decoupling Control of PMSM with SVR Inverse System Method'', the necessity of the feature weighting of inverse model is analyzed in theory, and then the realization of decoupling control of PMSM with feature weighting SVR inverse system method is introduced in detail. Simulation results and discussion are shown in Section 4 ''Simulation and Experiment Results''. In Section 5 ''Conclusions'', we come to a conclusion.

II. PRELIMINARIES

A. ANALYTIC INVERSE SYSTEM OF PMSM

PMSMs are classified into two typical types: surface-mounted PMSM and interior PMSM [19]. This article takes surface-mounted PMSM as the research object. The mathematical model for the original PMSM system based on the $d-q$ axis can be expressed as

$$\begin{cases} \dfrac{di_d}{dt} = \dfrac{1}{L}u_d - \dfrac{R}{L}i_d + i_q\omega_r \\ \dfrac{di_q}{dt} = \dfrac{1}{L}u_q - \dfrac{R}{L}i_q - i_d\omega_r - \dfrac{\psi_f}{L}\omega_r \\ \dfrac{d\omega_r}{dt} = \dfrac{3P_n^2\psi_f}{2J}i_q - \dfrac{P_nT_L}{J} \end{cases} \tag{1}$$

where u_d and u_q are the stator voltage of d-axis and q-axis respectively, i_d and i_q are the stator current of d-axis and q-axis respectively. R is the stator resistance, $L = L_d = L_q$ in which L_d and L_q are the inductance of d-axis and q-axis respectively, ω_r is the rotor electrical speed, ψ_f is the permanent magnet flux, P_n is the number of pole pairs, J is the moment of inertia of the rotor, and T_L is the load torque.

The original system of this article is built based on FOC in which the rotor electrical speed ω_r and stator current of d-axis i_d are decoupled. Therefore, $u = [u_1, u_2]^{\mathrm{T}} = [u_d, u_q]^T$ and $y = [y_1, y_2]^{\mathrm{T}} = [i_d, \omega_r]^T$ are chosen as the input and output variables of the original system. According to Eq.(1), i_d, i_q and ω_r are chosen as state variables $x = [x_1, x_2, x_3]^{\mathrm{T}} = [i_d, i_q, \omega_r]^T$. Based on the theory of inverse system and Interactor, output y_1 and output y_2 are differentiated until the results obviously contain input u_1 and input u_2 respectively.

$$\begin{cases} y_1' = \dfrac{1}{L}u_1 - \dfrac{R}{L}x_1 + x_2x_3 \\ y_2'' = \dfrac{3P_n^2\varphi_f}{2J}\left(\dfrac{1}{L}u_2 - \dfrac{R}{L}x_2 - x_1x_3 - \dfrac{\psi_f}{L}x_3\right) \end{cases} \tag{2}$$

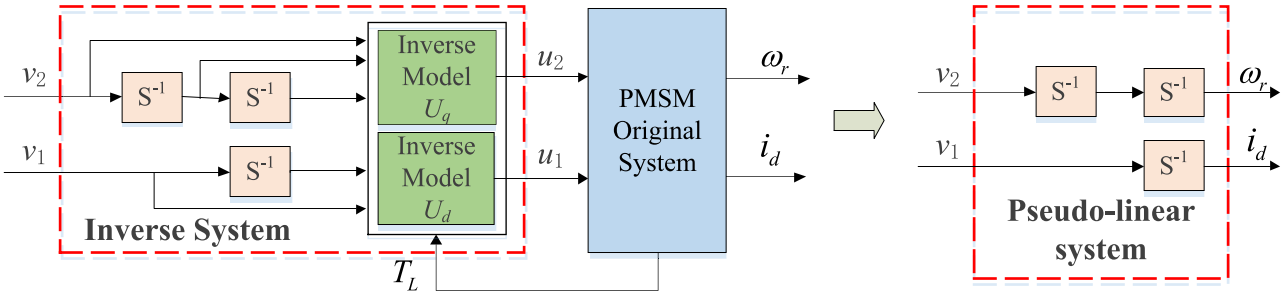

FIGURE 1. Diagram of pseudo-linear system based on analytical inverse system.

The inverse system will be cascaded with the original system. Therefore, the output of the inverse system is $u = [u_1, u_2]^{\mathrm{T}} = [u_d, u_q]^T$, which is the input of the original system. y_1' and y_2'' are chosen as the input $v = [v_1, v_2]^{\mathrm{T}} = [y_1', y_2'']^T = [i_d', \omega_r'']^T$. Consequently, the analytical inverse system derived from the mathematical model of PMSM can be expressed as

$$\begin{cases} u_1 = Lv_1 + Rx_1 - Lx_2x_3 \\ u_2 = \dfrac{2JL}{3p_n^2\psi_f}v_2 + Rx_2 + Lx_1x_3 + \psi_f x_3 \end{cases} \tag{3}$$

Eq.(3) can be rewritten as

$$\begin{cases} u_1 = Lv_1 + Rx_1 - \dfrac{2JLx_3}{3p_n^2\psi_f}\left(x_3' + \dfrac{p_nT_L}{J}\right) \\ u_2 = \dfrac{2JL}{3p_n^2\psi_f}v_2 + \dfrac{2JR}{3p_n^2\psi_f}\left(x_3' + \dfrac{p_nT_L}{J}\right) + Lx_1x_3 + \psi_f x_3 \end{cases} \tag{4}$$

Eq.(4) is equivalent to Eq.(5).

$$\begin{cases} u_d = Li'_d + Ri_d - \dfrac{2JL\omega_r}{3p_n^2\psi_f}\left(\omega_r' + \dfrac{p_nT_L}{J}\right) \\ u_q = \dfrac{2JL\omega_r''}{3p_n^2\psi_f} + \dfrac{2JR\omega_r'}{3p_n^2\psi_f} + \psi_f\omega_r + Li_d\omega_r + \dfrac{2RT_L}{3p_n\psi_f} \end{cases} \tag{5}$$

A new pseudo-linear system can be obtained by cascading the analytical inverse system with the original system. It is shown in Figure 1.

B. MODELING OF NONLINEAR SYSTEM BY USING SVR

The training dataset is given as $T = \{(x_i, y_i), i = 1, \ldots l\}$, where $x_i \in R^n$ is the i-th input sample containing n features and $y_i \in R$ is the output. The model function determined by SVR method is expressed as follows:

$$f(x) = < w, \phi(x) > + b \tag{6}$$

where $w \in R^n$ is a weight vector of hyperplane,$\phi(x)$ maps the samples of input features to a high-dimensional kernel space, and b is a bias term.

The model function Eq.(6) can be further developed as follows:

$$f(x) = \sum_{i=1}^{l}(\bar{\alpha}_i^* - \bar{\alpha}_i)K(x_i, x) + \bar{b} \tag{7}$$

where K is the kernel matrix. K can be expressed as follows when Gaussian kernel is selected.

$$K(x_i, x_j) = \exp\left(-\gamma\left(\sum_{k=1}^{n}(x_{ik} - x_{jk})^2\right)\right) \tag{8}$$

III. DECOUPLING CONTROL OF PMSM WITH SVR INVERSE SYSTEM METHOD

A. MODELING OF INVERSE SYSTEM USING SVR

The training set of inverse model U_d is given as $T_d = \{(x_j^d, y_j^d), j = 1, \ldots l\}$, where $x_j^d = [i_d(j), i_d'(j), \omega_r(j), \omega_r'(j), T_L(j)]^{\mathrm{T}}$ is the j-th input sample containing five features and $y_j^d = u_d(j)$ is the j-th output sample. The training set of inverse model U_q is given as $T_q = \{(x_j^q, y_j^q), j = 1, \ldots l\}$, where $x_j^q = \left[\omega_r(j), \omega_r'(j), \omega_r''(j), i_d(j), T_L(j)\right]^{\mathrm{T}}$ is the input sample containing five features and $y_j^q = u_q(j)$ is the output sample. The training samples $i_d, \omega_r, T_L, u_d, u_q$ are sampled from the closed-loop control system of PMSM based on the analytical inversion, and $i_d', \omega_r', \omega_r''$ are calculated by using the five-point numerical differential method.

The inverse model U_q is used as an example to analyze the influence of input features on kernel space feature as follows. It won't hurt to assume that $T_L = 0$.

$$u_q = \frac{2JL\omega_r''}{3p_n^2\psi_f} + \frac{2JR\omega_r'}{3p_n^2\psi_f} + \psi_f\omega_r + Li_d\omega_r \tag{9}$$

Let's assume $R = 0.958\Omega$, $L = L_d = L_q = 8.35 \times 10^{-4}$H, $J = 8.35 \times 10^{-3}$kg $\cdot$ m^2, $Pn = 4$, $\psi_f = 0.1827$Wb, Eq.(9) can be rewritten as

$$u_q = (5.7129\text{e-}7)\omega_r'' + (6.5545\text{e-}04)\omega_r' + 0.1827\omega_r + (8.3500\text{e-}04)i_d\omega_r \tag{10}$$

The similarity between x_i^q and x_j^q in kernel space can be obtained by calculating the distance d_{jk} between the maps of two samples in kernel space.

$$\begin{aligned} d_{jk} &= \left\|\phi\left(x_j^q\right) - \phi\left(x_k^q\right)\right\|^2 \\ &= \left\langle\phi\left(x_j^q\right) - \phi\left(x_k^q\right), \phi\left(x_j^q\right) - \phi\left(x_k^q\right)\right\rangle \\ &= \left\langle\phi\left(x_j^q\right), \phi\left(x_j^q\right)\right\rangle - 2\left\langle\phi\left(x_j^q\right), \phi\left(x_k^q\right)\right\rangle \end{aligned}$$

$$
\begin{aligned}
&+\left\langle \phi\left(x_k^q\right), \phi\left(x_k^q\right)\right\rangle \\
&= K\left(x_j^q, x_j^q\right) - 2K\left(x_j^q, x_k^q\right) + K\left(x_k^q, x_k^q\right) \\
&= 2 - 2\exp\left(-\gamma\left\|x_j^q - x_k^q\right\|^2\right) \\
&= 2-2\exp\left(-\gamma\left(\begin{array}{c}(\omega_r(j)-\omega_r(k))^2+\left(\omega_r'(j)-\omega_r'(k)\right)^2 \\ +\left(\omega_r''(j)-\omega_r''(k)\right)^2+(i_d(j)-i_d(k))^2\end{array}\right)\right)
\end{aligned} \tag{11}
$$

In steady operation condition, u_q is mainly determined by ω_r because ω_r', ω_r'' and i_d are all tend to zero. The approximations of u_q and d_{jk} can be expressed as

$$
\begin{cases} u_q \approx 0.1827\omega_r \\ d_{jk} \approx 2 - 2\exp\left(-\gamma\left(\omega_r(j) - \omega_r(k)\right)^2\right) \end{cases} \tag{12}
$$

It can be seen from Eq.(12) that the rotor electrical speed ω_r has the greatest influence on the output of inverse model U_q and the similarity of samples in kernel space.

In transient operation condition, the value of ω_r'' may be 10^7 level, the value of ω_r' may be 10^4 level, and the value of ω_r may be 10^3 level. According to Eq.(10), the coefficients of input features ω_r'' and ω_r' are 5.7129e - 7 and 6.5545e - 04 respectively; the third item and fourth can be combined and written as $(0.1827 + (8.3500\text{e} - 04)i_d)\,\omega_r$, so the coefficient of ω_r can be approximately taken as 0.1827 and i_d has slight effect on the output u_q. For the similarity of samples in kernel space, input feature ω_r'' has the greatest influence on the similarity of kernel space because of its great advantage in magnitude. Therefore, the approximation of u_q and d_{jk} in transient operation conditions can be expressed as

$$
\begin{cases} u_q \approx (5.7129\text{e} - 7)\omega_r'' + (6.5545\text{e} - 04)\omega_r' + 0.1827\omega_r \\ d_{jk} \approx 2 - 2\exp\left(-\gamma\left(\omega_r''(j) - \omega_r''(k)\right)^2\right) \end{cases} \tag{13}
$$

It can be seen from Eq. (13) that the contribution of input features to the construction of kernel space does not match their contribution to output u_q. Therefore, it is unreasonable to use the raw data of input features to construct the kernel space of inverse model. Similarly, feature normalization also can not solve it.

Feature weighting can make the contribution of input features to the construction of kernel space match their contribution to the output.The conventional SVR model Eq.(6) can be further developed to feature weighting SVR(FW-SVR) as follows:

$$
f(x) = \sum_{i=1}^{l}\left(\bar{\alpha}_i^* - \bar{\alpha}_i\right)K_{\varpi}(x_i, x) + \bar{b} \tag{14}
$$

where K_{ϖ} is the weighted kernel matrix and K_{ϖ} can be expressed as

$$
K_{\varpi}(x_i, x_j) = \exp\left(-\gamma\left(\sum_{k=1}^{n}\left(\varpi_k\left(x_{ik} - x_{jk}\right)\right)^2\right)\right) \tag{15}
$$

where ϖ_k is the weight value of k-th input feature.

After the feature weights $\varpi^q = \left[\varpi_1^q, \varpi_2^q, \varpi_3^q, \varpi_4^q\right]^{\mathrm{T}}$ are introduced into the calculation of kernel elements, d_{jk} can be expressed as follows:

$$
d_{jk} = 2-2\exp\left(-\gamma\left(\begin{array}{c}\left(\varpi_1^q\left(\omega_r(j) - \omega_r(k)\right)\right)^2 \\ +\left(\varpi_2^q\left(\omega'_r(j) - \omega'_r(k)\right)\right)^2 \\ +\left(\varpi_3^q\left(\omega''_r(j) - \omega''_r(k)\right)\right)^2 \\ +\left(\varpi_4^q\left(i_d(j) - i_d(k)\right)\right)^2\end{array}\right)\right) \tag{16}
$$

The feature weights can be adjusted to a reasonable value so that the influence of input features on sample similarity in kernel space matches with that on output u_q, which makes the kernel space feature of SVR inverse model more reasonable.

Therefore, the inverse model U_q based on FW-SVR can be expressed as

$$
f_q(x) = \sum_{j=1}^{l}\left(\bar{\alpha}_{qj}^* - \bar{\alpha}_{qj}\right)K_{q\varpi}\left(x_j^q, x\right) + b_q \tag{17}
$$

Similarly, the inverse model U_d based on FW-SVR can be expressed as

$$
f_d(x) = \sum_{j=1}^{l}\left(\bar{\alpha}_{dj}^* - \bar{\alpha}_{dj}\right)K_{d\varpi}\left(x_j^d, x\right) + b_d \tag{18}
$$

According to the coefficients of each item in Eq.(4) and considering the operation condition of PMSM, the value of ϖ^d and ϖ^q are given as follows:

$$
\begin{cases}
\varpi^d = \left[\varpi_1^d, \varpi_2^d, \varpi_3^d, \varpi_4^d, \varpi_5^d\right]^{\mathrm{T}} \\
\quad = \left[R, L, -\dfrac{2JL\xi_1}{3p_n^2\psi_f}, -\dfrac{2JL\xi_2}{3p_n^2\psi_f}, -\dfrac{2L\xi_2}{3p_n\psi_f}\right]^{\mathrm{T}} \\
\varpi^q = \left[\varpi_1^q, \varpi_2^q, \varpi_3^q, \varpi_4^q, \varpi_5^q\right]^{\mathrm{T}} \\
\quad = \left[\psi_f, \dfrac{2JR}{3p_n^2\psi_f}, \dfrac{2JL}{3p_n^2\psi_f}, L\xi_3, \dfrac{2R}{3p_n\psi_f}\right]^{\mathrm{T}}
\end{cases} \tag{19}
$$

where ξ_1, ξ_2 and ξ_3 are empirical parameters which are specified on operation conditions of PMSM in analytical inverse system.

B. CONTROL SYSTEM OF PMSM BASED ON FW-SVR INVERSE SYSTEM METHOD

As the size of sample is limited, the training sample can not contain all operation conditions and the PMSM parameters will change under the influence of various factors. Therefore, the open-loop pseudo-linear system by cascading the inverse system with the original system can not achieve high performance. In this article, PID controller is used to overcome the disturbances from both internal and external. The diagram of PID control system is shown in Figure 2.

C. STEPS OF INVERSE SYSTEM METHOD BASED ON FW-SVR

1. Design a sampling system for training dataset. The pseudo-linear system shown in Figure 1 is combined with PID controller to form a closed-loop control system and the

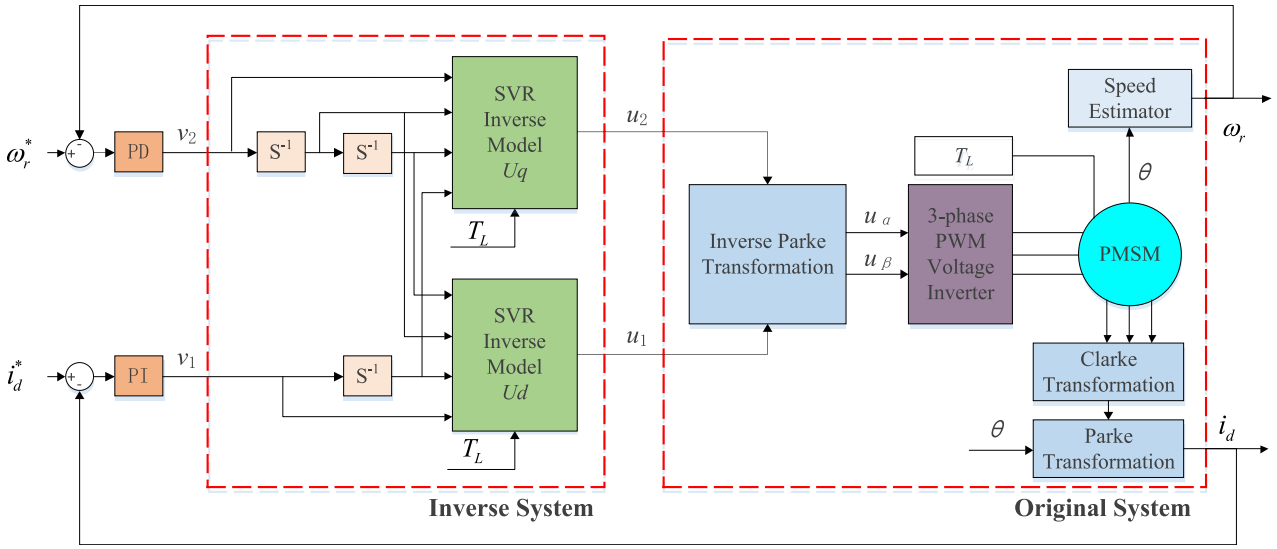

FIGURE 2. Control diagram of the PMSM based on FW-SVR inverse system method.

parameters of PID are adjusted to make the analytical inverse control system run normally.

2. Obtain the training samples. $i_d, \omega_r, T_L, u_d, u_q$ are sampled and $i_d', \omega_r', \omega_r''$ are calculated by five-point numerical differentiation method to form training sets T_d and T_q.

3. Select the optimal combination of feature weights, which are based on operation conditions and PMSM parameters.

4. Build a inverse system based on FW-SVR. Select parameters (C, γ, ε) for model U_d and U_q and train two FW-SVR inverse models by utilizing the obtained optimal model parameters.

5.Design a control system. When the inverse system cascades with the original system, the PMSM system is decoupled into two pseudo-linear subsystems. The control system shown in Figure 2 is established.

6.Adjust the PID controller parameters in Figure 2 to realize high-performance closed-loop control of PMSM.

IV. SIMULATION AND EXPERIMENT RESULTS

Comparative simulation between the proposed FW-SVR and the traditional SVR is carried out to prove the feasibility of the FW-SVR inverse system.Root mean square error (RMSE) is employed to evaluate the feasibility of FW-SVR.

$$\mathrm{RMSE} = \sqrt{\frac{1}{l}\sum_{i=1}^{l}[u_i - f(x_i)]^2} \tag{20}$$

where u_i is the output sample and $f(x_i)$ is its predicted value. The smaller the value of RMSE, the better the generalization ability of the model.

The datasets T_1 and T_2 generated under different excitation signals are sampled for convenient comparision.The training set of the two models are both composing of 501 samples taken at equal intervals from T_1. For model U_d and model U_q, the training set is T_d and T_q respectively.The input feature ω_r, ω_r', ω_r'',i_d, i_d' in T_d and T_q is shown in Figure 3. The output u_d in T_d and the output u_q in T_q are shown in Figure 4.

A. KERNEL SPACE FEATURE

The kernel matrix can fully reflect the similarity between samples in kernel space. The inverse model U_q is taken as an example and the kernel parameter γ is set to 1×10^{-10} for convenient observation. The influence of input features such as ω_r'', ω_r', ω_r, i_d on kernel space similarity is shown in Figure 5.

As can be seen from Figure 5, Figure 5(a) and Figure 5(b) are the closest, indicating that the kernel space similarity is mainly affected by input feature ω_r'' unreasonably. First of all, although the amplitude of input feature ω_r'' is large, it doesn't contribute a lot to the output of the model. When working on the output, ω_r'' is multiplied by the coefficient $2JL/3p_n^2\psi_f$ which is a small value of 5.7129e-07 in this article. On the contrary, although the amplitude of ω_r is smaller than that of ω_r'', its contribution is larger than that of ω_r'' after it multiplies the coefficient $\left(\psi_f + Li_d\right) = (0.1827 + (8.35\mathrm{e}-4)\, i_d) \approx 0.1827$. Therefore, kernel space feature represented by the similarity of samples are unreasonable when the contribution of input features to the output is not considered and raw data or normalized data is used for model training.

B. GENERALIZATION ABILITY OF FW-SVR INVERSE MODEL

There are two kinds of model test sets: one comes from the same sample set as the training set does, and the other from different sample set. For model U_d, the test sets are S_{d1} from T_1 and S_{d2} from T_2. For model U_q, the test sets are S_{q1} from T_1 and S_{q2} from T_2.

In this article, ξ_1, ξ_2 and ξ_3 are set to 1e-4, 1e-3 and 1e-3 respectively when both the Eq. (4) and the operation

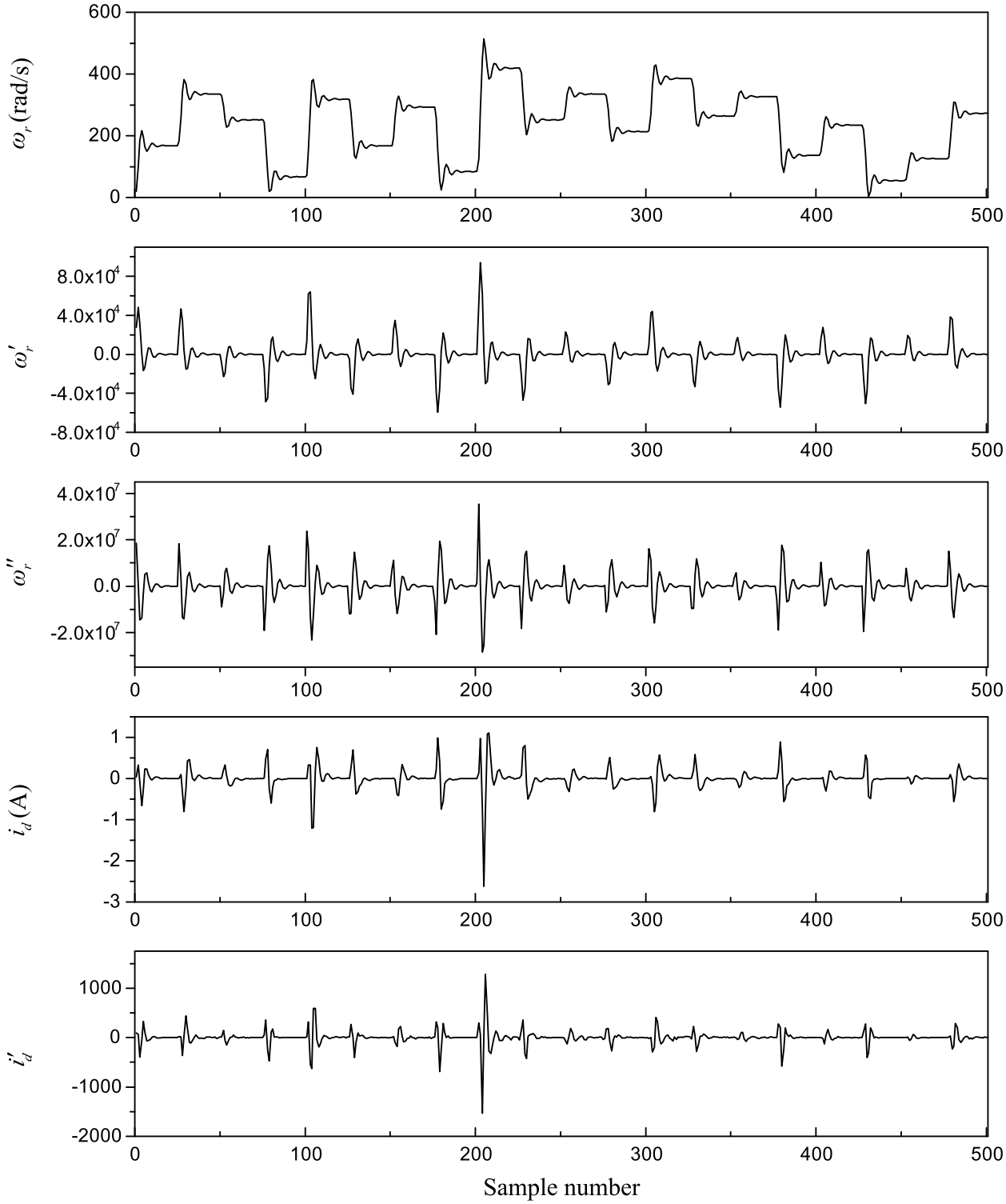

FIGURE 3. The input features of sample set T_1: i_d, i'_d, ω_r and ω'_r are the input features of inverse model U_d; ω_r, ω'_r, ω''_r and i_d are the input features of inverse model U_q.

conditions of analytical inverse system are taken into account. The values of ϖ^d and ϖ^q are given as follows:

$$\begin{cases} \varpi^d = [0.958, 8.35\text{e-}4, -0.0057, -5.7129\text{e-}4, -0.7617]^{\mathrm{T}} \\ \varpi^q = [0.1827, 6.5545\text{e-}4, 5.7129\text{e-}7, 0.835, 0.8739]^{\mathrm{T}} \end{cases} \tag{21}$$

The difference of the model generalization ability under different feature weights is shown by an example about model U_q to verify the necessity of feature weighting. Firstly, the weight ϖ_1^q and weight ϖ_4^q of the first input feature ω_r and the fourth input feature i_d are selected to be analyzed. Then, ϖ_1^q and ϖ_4^q are multiplied by the specified coefficients

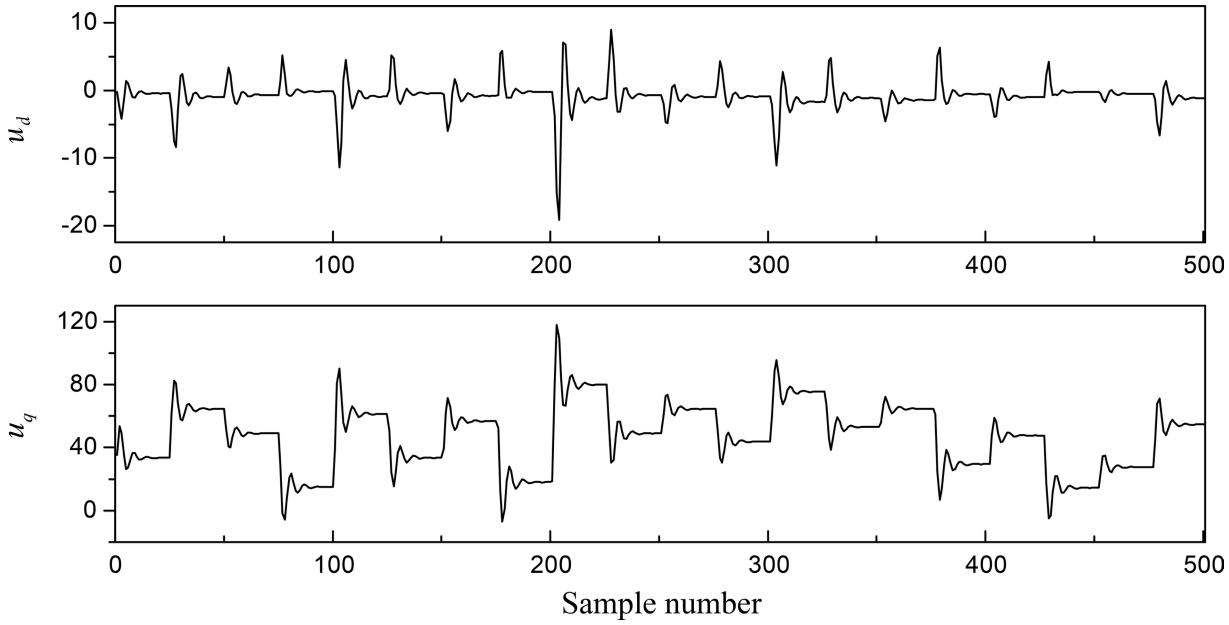

FIGURE 4. The output features of sample set T_1: u_d is the output feature of inverse model U_d; u_q is the output feature of inverse model U_q.

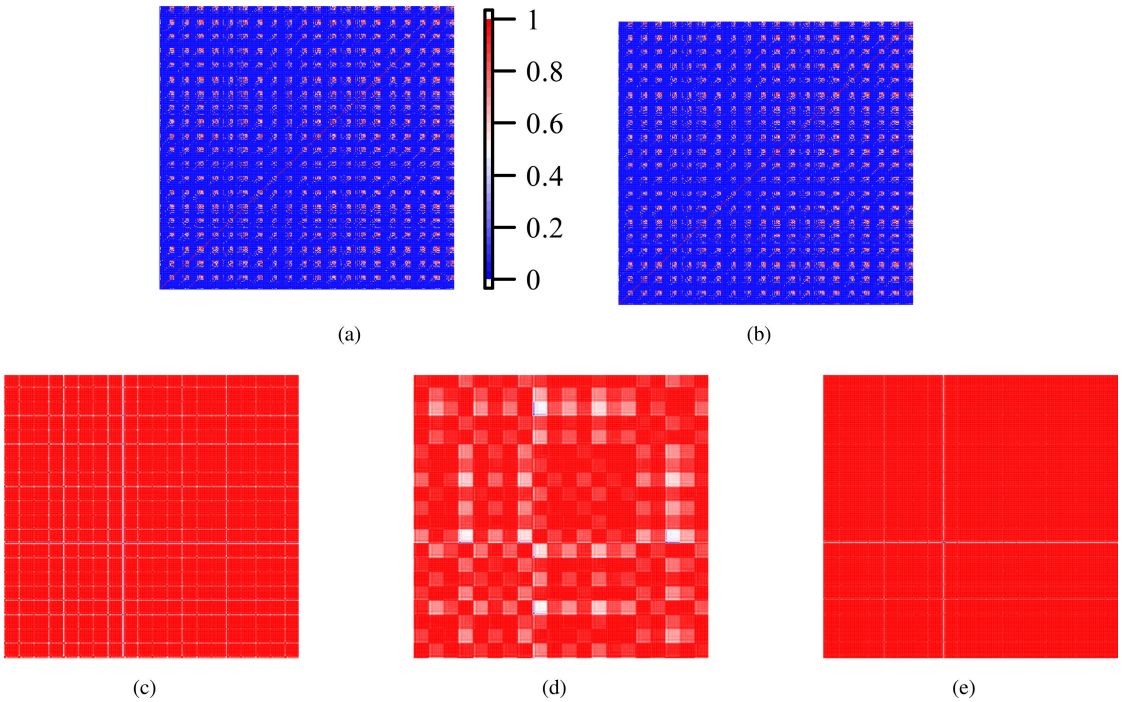

FIGURE 5. Five 2D heat-maps of kernel matrices: (a) kernel matrix generated by all five input features; (b) kernel matrix generated by input feature ω_r''; (c) kernel matrix generated by input feature ω_r'; (d) kernel matrix generated by input feature ω_r; (e) kernel matrix generated by input feature i_d.

to form a new ϖ^q for training the model. Finally, RMSE is obtained after the model is tested with test set S_{q2}. The coefficients of ϖ_1^q are from set $\{2^{-9}, 2^{-8}, 2^{-7}, \cdots, 2^7\}$ and those of ϖ_4^q are from set $\{2^{-10}, 2^{-9}, 2^{-8}, \cdots, 2^{10}\}$.Therefore, 357 RMSEs for each possible combination of ϖ_1^q and ϖ_4^q are obtained. The model performance is shown as Figure 6 accordingly.

As can be seen from Figure 6, the generalization ability of inverse model U_q is obviously affected by the feature weights. For feature ϖ_1^q, the generalization ability is very poor when its coefficient is less than 2^{-5} or greater than 2^5. For feature ϖ_4^q, the generalization ability is very poor when its coefficient is greater than 2^6 while RMSE does not increase significantly when the coefficient gradually decreases to 2^{-10}. The feature

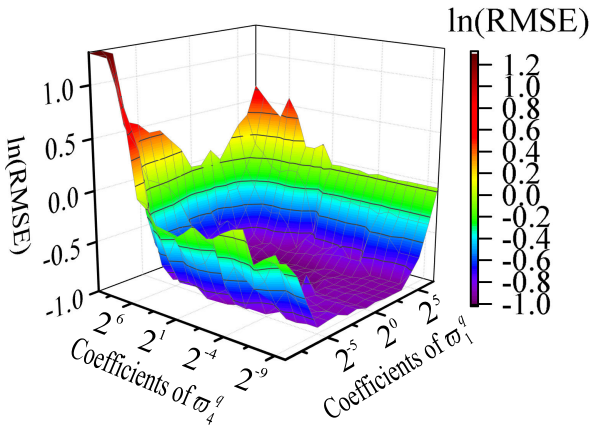

FIGURE 6. Model generalization ability of different weights combination of ϖ_3^q and ϖ_4^q.

1 of model U_q is ω_r which has an important contribution to output according to Eq. 5. Therefore, the influence of input features on the sample similarity in kernel space will not match with that on output u_q, which makes the kernel space feature of inverse model U_q is not reasonable until ϖ_1^q is adjusted to a reasonable value. Feature 4 is i_d which corresponds to $L\omega_r i_d$ of the fourth term of U_q. Even if ω_r is the maximum value in training sample, i_d has slight effect on output. Therefore, RMSE does not increase greatly with the decrease of the coefficient of ϖ_4^q. In addition, it can be seen from Figure 6 that the selection range of feature weights is large, and the generalization ability of the inverse model U_q can be guaranteed as long as it is within a reasonable range.

The proposed FW-SVR is compared with feature normalization SVR(FN-SVR) and raw dataset SVR(RD-SVR) to observe the generalization difference of U_d and U_q.

Firstly, test sets S_{d1} and S_{q1} from the same sampling dataset T_1 as training sets T_d and T_q are used to test U_d and U_q models respectively. The predicted output of the models is shown in Figure 7.

Then, training dataset and test dataset are taken from different sample sets. For model U_d, training dataset is T_d and test dataset S_{d2}; for model U_q, training dataset T_q and test dataset S_{q2}.The predicted output of the model is shown in Figure 8.

RMSEs of the test set S_{d1}, S_{d2}, S_{q1} and S_{q2} in Figure 7 and Figure 8 are given in Table 1.

As can be seen from Table 1, the performance of FW-SVR is the best; that of RD-SVR is the worst on all test sets; that of FN-SVR is good when the training set and test set are from the same sampling dataset, but it becomes worse for test samples from the new sampling dataset. For example, in U_d model, RMSE is 0.0160 when test set is S_{d1}, but it is 1.5394 when test set is S_{d2}. In U_q model, when the test set is S_{q1} and S_{q2}, RMSE is 0.1012 and 8.1999 respectively.

20 different test datasets are used to test U_d and U_q in order to further verify the performance of FW-SVR and FN-SVR on different test sets. The mean values and standard deviations of RMSEs are given in Table 2.

TABLE 1. Performance comparison of SVR modeling of test set S_{d1}, S_{d2}, S_{q1} and S_{q2}.

Model name	Test set	Method name	RMSE
U_d	S_{d1}	RD-SVR	1.4116
		FN-SVR	0.0160
		proposed FW-SVR	0.0246
	S_{d2}	RD-SVR	1.8585
		FN-SVR	1.5394
		proposed FW-SVR	0.0350
U_q	S_{q1}	Raw data	20.3031
		FN-SVR	0.1012
		proposed FW-SVR	0.1217
	S_{q2}	RD-SVR	22.0123
		FN-SVR	8.1999
		proposed FW-SVR	0.1277

TABLE 2. Performance comparison of SVR modeling for 20 different test sets.

Model name	Method name	RMSE(mean±Std)
U_d	FN-SVR	2.8268±2.0055
	proposed FW-SVR	0.0384±0.0232
U_q	FN-SVR	17.3876±11.0969
	proposed FW-SVR	0.1209±0.0237

Finally, the Wilcoxon signed rank test [20] at the 0.05 significance level is implemented to further explain the indications in Table 2. The test results are presented in Table 3.

TABLE 3. Wilcoxon signed rank test for the prediction results.

Model name	$p-value$
U_d	8.8575e-05
U_q	8.8575e-05

It can be seen from Table 2-3 that there is statistically significant difference between FW-SVR and FN-SVR and the performance of FW-SVR is better than that of FN-SVR in U_d and U_q test.

C. DECOUPLING CONTROL OF PMSM

In order to verify the effectiveness of the proposed FW-SVR inverse system method, analytical inverse system method and FN-SVR inverse method are compared with it.

As the analytical inverse method greatly depends on motor parameters, two sets of parameters are used to test the method. One is the correct parameters which is completely consistent with that in the original system, which can verify the effectiveness of the inverse system theory in PMSM control; the other that is not completely consistent with the parameters of the original system is used to observe the influence of inaccurate parameter measurement or parameter change during motor operation on control performance, which can explain the necessity of using SVR algorithm that is independent of parameters. The FW-SVR inverse system method and FN-SVR inverse system method are based on the structure of Figure 2. The initial reference speed is set to 400 rpm, rising to 800 rpm at 0.3 s and decreasing to 600 rpm at 0.6 s.

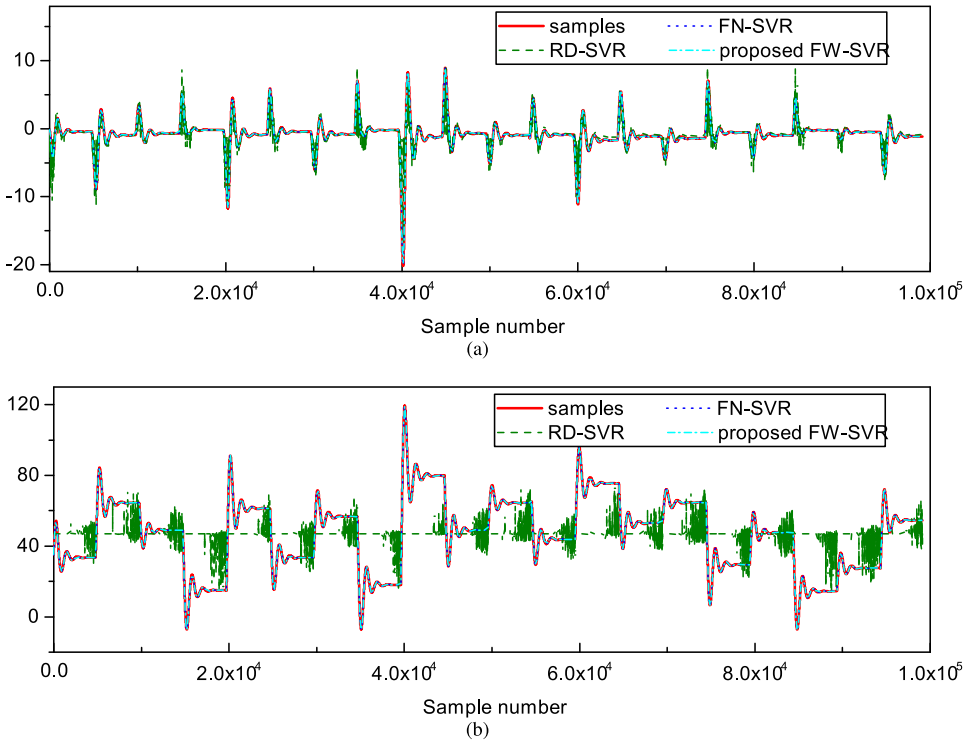

FIGURE 7. The predicted output for test set T_d and T_q: (a) The u_d predicted output for test set S_{d1}; (b) The u_q predicted output for test set S_{q1}.

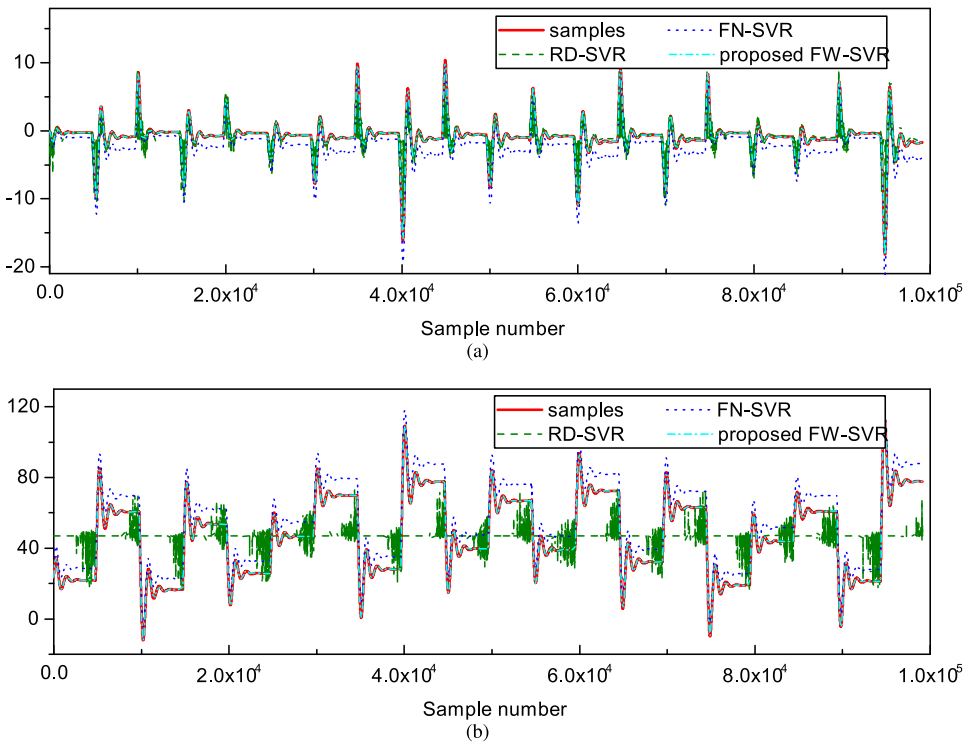

FIGURE 8. The predicted output for test set T_d and T_q: (a) The u_d predicted output for test set S_{d2}; (b) The u_q predicted output for test set S_{q2}.

1) SIMULATION RESULTS

The parameters of the motor are $R = 0.958\Omega$, $L = L_d = L_q = 8.35 \times 10^{-4}$H, $J = 8.35 \times 10^{-3}$kg $\cdot$ m^2, $Pn = 4$, $\psi_f = 0.1827$Wb. The initial load is 5 Nm, increasing to 7 Nm at 0.8 s. The fast response of speed and the influence of sudden change of load on speed stability are taken as the

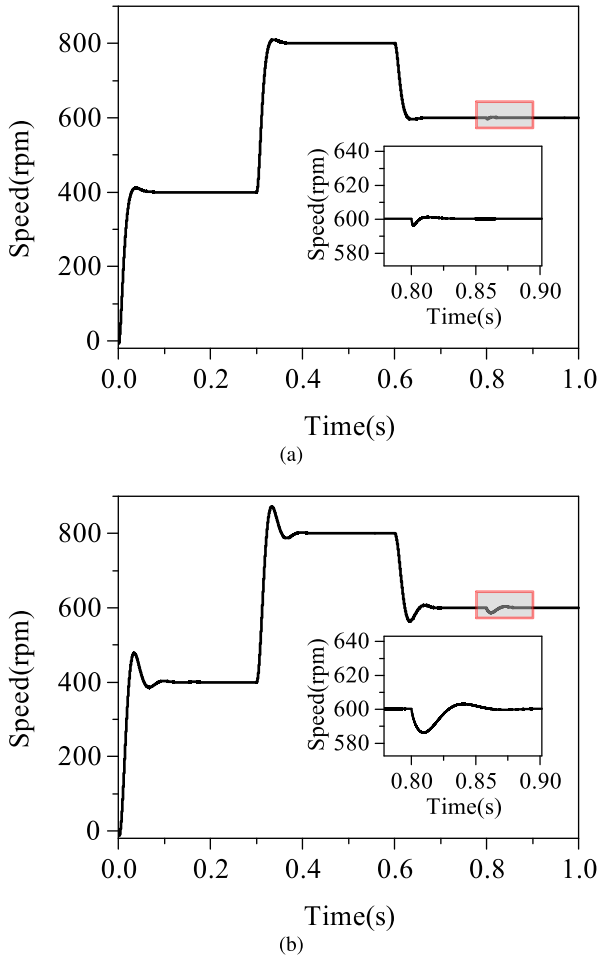

FIGURE 9. Simulated speed response of analytical inverse method: (a) the parameters set $R = 0.958\Omega$, $L = 8.35 \times 10^{-4}$H, $J = 8.35 \times 10^{-3}$kg · m^2, $Pn = 4$, $\psi_f = 0.1827$Wb in the analytical inverse system are completely consistent with that in the original system; (b) the parameters in the analytical inverse system are not completely consistent with that in the original system. The motor parameters in the analytical inverse system are $R = 0.958\Omega$, $L = 8.35 \times 10^{-4}$H, $J = 8.35 \times 10^{-3}$kg · m^2, $Pn = 4$ and $\psi_f = 0.1827$Wb; the parameters in the original system are $R = 1.437\Omega$, $L = 7.52 \times 10^{-4}$H, $J = 8.35 \times 10^{-3}$kg · m^2, $Pn = 4$ and $\psi_f = 0.1462$Wb.

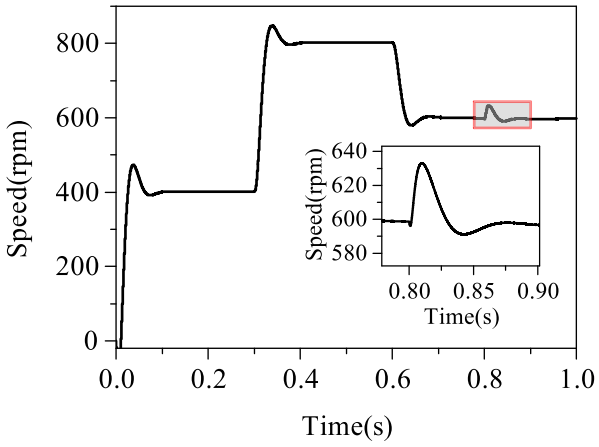

FIGURE 10. Simulated speed response of FN-SVR inverse method.

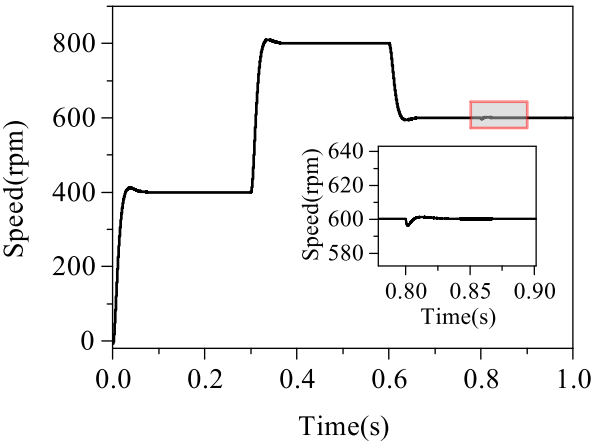

FIGURE 11. Simulated speed response of the proposed FW-SVR inverse method.

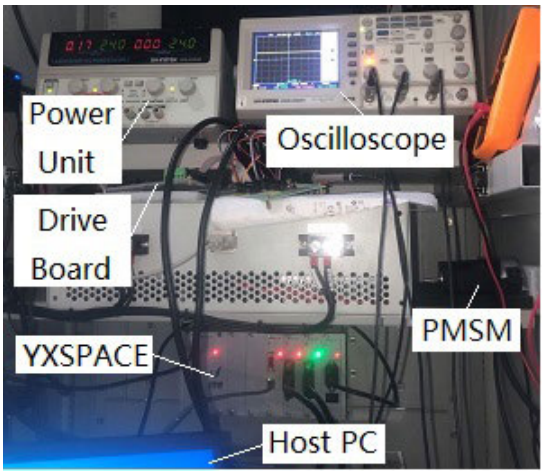

FIGURE 12. Experiment platform.

evaluation indexes of decoupling control performance. The control performance is shown in Figure 9-11.

It can be seen from Figure 9-11 that FW-SVR inverse system method proposed in this article achieves the best control performance. As shown in Figure 9(a), when the motor parameters are completely consistent with the actual parameters, the analytical inverse system method achieves the same control performance as the FW-SVR inverse system method. However, in Figure 9(b), when motor parameters used in analytical inverse system are different from the actual ones, its performance is shown as follows: the overshoot is 78.5 rpm when the motor starts, it is 72.6 when the speed increases from 400 rpm to 800 rpm and it is 35.6 when the speed decreases from 800 rpm to 600 rpm; the speed decreases from 600 rpm to 586.2 rpm when the load jumps from 5 Nm to 7 Nm and it returns to a steady state 0.06 second later. In general, the inverse system method is feasible in PMSM control on condition that the inverse model is accurate enough to ensure the decoupling control performance after overcoming the dependence on parameters.

As shown in Figure 10, although FN-SVR does not rely on motor parameters, its decoupling control performance is not good because the model is not accurate enough. As shown

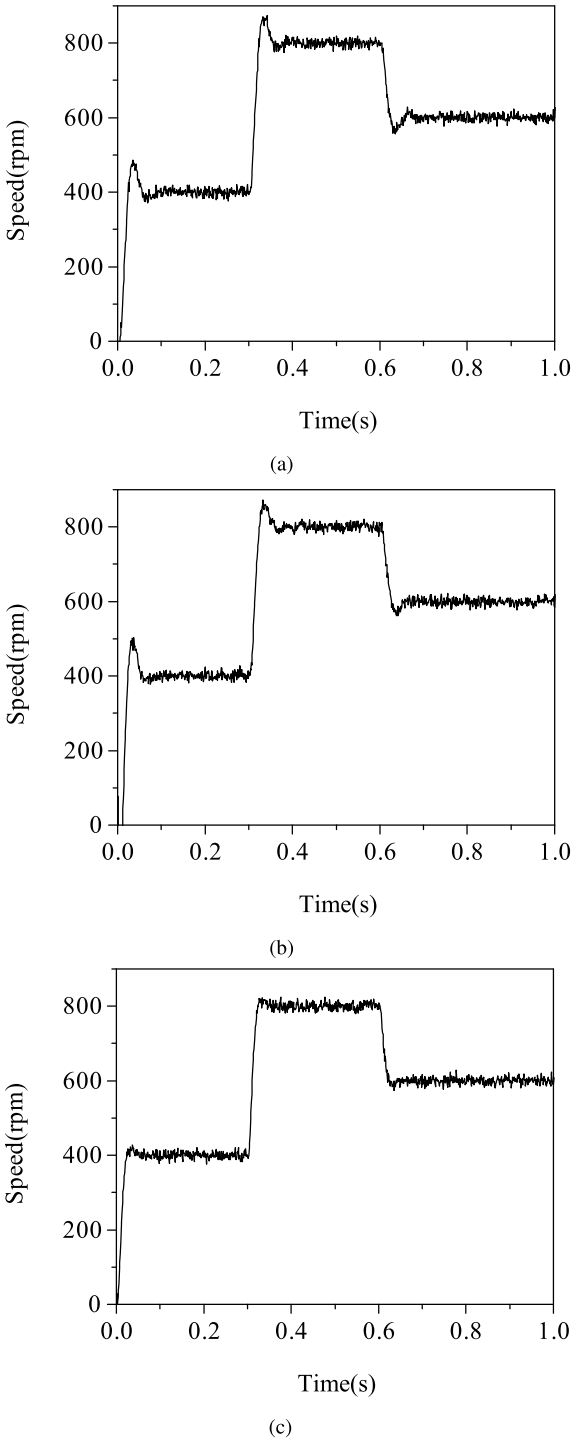

FIGURE 13. Experiment results. (a) Speed response of analytical inverse method: the parameters set $R = 0.900\Omega, J = 6.30 \times 10^{-4}\text{kg} \cdot \text{m}^2$, $L = L_d = L_q = 6.25 \times 10^{-4}\text{H}, Pn = 4$, $\psi_f = 0.01585\text{Wb}$; (b) Speed response of FN-SVR inverse method; (c) Speed response of the proposed FW-SVR inverse method.

in Figure 11, the maximum overshoot is 11.5 rpm and the motor speed only decreases 3.7 rpm when the load is disturbed. As the FW-SVR inverse system method does not only overcome the dependence on motor parameters, but also build an accurate inverse model by optimizing the kernel space features, its decoupling control performance is the best.

2) EXPERIMENT RESULTS

The experiments which are based on YXSPACE-10 rapid controller prototyping are performed for further verification. The experiment platform is designed as Figure 12.

The parameters of the motor are $R = 0.900\Omega$, $L = L_d = L_q = 6.25 \times 10^{-4}\text{H}$, $Pn = 4$, $J = 6.30 \times 10^{-4}\text{kg} \cdot \text{m}^2$ and $\psi_f = 0.01585\text{Wb}$. The load is 0.2Nm. The fast response of the speed is taken as the evaluation indexes of control performance. The control performance is shown in Figure 13.

It can be seen from Figure 13 that the speed response of FW-SVR inverse system method proposed in this article achieves the best performance. In Figure 13(a), the performance of analytical inverse system method is shown as follows: the overshoot is 86.4 rpm when the motor starts, it is 74.2 when the speed increases from 400 rpm to 800 rpm and it is 43.9 when the speed decreases from 800 rpm to 600 rpm. As shown in Figure 13(b), the performance of FN-SVR inverse system method is similar to that of analytical inverse system method. As shown in Figure 13(c), the maximum overshoot is 27.5 rpm.

V. CONCLUSION

In this article, a novel FW-SVR inverse system method is proposed for decoupling control of PMSM. The contribution of input features to the construction of kernel space is estimated based on the mathematical model of analytical inverse system. Therefore, the feature weights of FW-SVR can be adjusted to a reasonable value which makes the kernel space feature of SVR inverse model more reasonable.The comparative simulation and experiment results demonstrate that: (1) The generalization ability of SVR inverse model is obviously affected by the feature weights while it can be improved by FW-SVR; (2) The FW-SVR inverse system method is feasible in decoupling control of PMSM because it does not only overcome the dependence on motor parameters, but also build an accurate inverse model.

REFERENCES

[1] P. T. Luu, J.-Y. Lee, J.-H. Lee, and J.-W. Park, "Electromagnetic and thermal analysis of permanent-magnet synchronous motors for cooperative robot applications," *IEEE Trans. Magn.*, vol. 56, no. 3, pp. 1–4, Mar. 2020.

[2] X. Sun, Z. Shi, G. Lei, Y. Guo, and J. Zhu, "Analysis and design optimization of a permanent magnet synchronous motor for a campus patrol electric vehicle," *IEEE Trans. Veh. Technol.*, vol. 68, no. 11, pp. 10535–10544, Nov. 2019.

[3] A. A. Adly and A. Huzayyin, "The impact of demagnetization on the feasibility of permanent magnet synchronous motors in industry applications," *J. Adv. Res.*, vol. 17, pp. 103–108, May 2019.

[4] J. Rodriguez, R. M. Kennel, J. R. Espinoza, M. Trincado, C. A. Silva, and C. A. Rojas, "High-performance control strategies for electrical drives: An experimental assessment," *IEEE Trans. Ind. Electron.*, vol. 59, no. 2, pp. 812–820, Feb. 2012.

[5] L. A. Adase, I. M. Alsofyani, and K.-B. Lee, "Predictive torque control with simple duty-ratio regulator of PMSM for minimizing torque and flux ripples," *IEEE Access*, vol. 8, pp. 2373–2381, 2020.

[6] D. Casadei, F. Profumo, G. Serra, and A. Tani, "FOC and DTC: Two viable schemes for induction motors torque control," *IEEE Trans. Power Electron.*, vol. 17, no. 5, pp. 779–787, Sep. 2002.

[7] X. Sun, B. Su, L. Chen, Z. Yang, X. Xu, and Z. Shi, "Precise control of a four degree-of-freedom permanent magnet biased active magnetic bearing system in a magnetically suspended direct-driven spindle using neural network inverse scheme," *Mech. Syst. Signal Process.*, vol. 88, pp. 36–48, May 2017.
[8] J.-F. Mao, G.-Q. Wu, A.-H. Wu, and X.-D. Zhang, "Nonlinear decoupling sliding mode control of permanent magnet linear synchronous motor based on α-th order inverse system method," in *Proc. Int. Conf. Adv. Control Eng. Inf. Sci. (CEIS)*, in Procedia Engineering, vol. 15, C. Ran and G. Yang, Eds. Norager, Denmark: Dali, Peoples R China, Aug. 2011, pp. 561–567.
[9] X. Li, Y. Wu, S. Shen, and X. Zhao, "The inverse system decoupling control of the permanent magnet synchronous motor in D-q synchronous rotating reference frame," *Procedia Eng.*, vol. 24, pp. 78–82, Jan. 2011.
[10] G. Liu, L. Chen, W. Zhao, Y. Jiang, and L. Qu, "Internal model control of permanent magnet synchronous motor using support vector machine generalized inverse," *IEEE Trans. Ind. Informat.*, vol. 9, no. 2, pp. 890–898, May 2013.
[11] Y. He and Z. Wang, "High-performance control of high-speed permanent magnet synchronous motor based on least squares support vector machine inverse system method," *Electr. Power Compon. Syst.*, vol. 45, no. 1, pp. 99–110, Jan. 2017.
[12] X. Sun, L. Chen, H. Jiang, Z. Yang, J. Chen, and W. Zhang, "High-performance control for a bearingless permanent-magnet synchronous motor using neural network inverse scheme plus internal model controllers," *IEEE Trans. Ind. Electron.*, vol. 63, no. 6, pp. 3479–3488, Jun. 2016.
[13] S. Salcedo-Sanz, J. L. Rojo-Álvarez, M. Martínez-Ramón, and G. Camps-Valls, "Support vector machines in engineering: An overview," *Wiley Interdiscipl. Rev., Data Mining Knowl. Discovery*, vol. 4, no. 3, pp. 234–267, May 2014.
[14] E. Pourjafari and M. Reformat, "A support vector regression based model predictive control for volt-var optimization of distribution systems," *IEEE Access*, vol. 7, pp. 93352–93363, 2019.
[15] A. J. Smola and B. Schölkopf, "A tutorial on support vector regression," *Statist. Comput.*, vol. 14, no. 3, pp. 199–222, Aug. 2004.
[16] M. Paliwal and U. A. Kumar, "Review: Neural networks and statistical techniques: A review of applications," *Expert Syst. Appl.*, vol. 36, no. 1, pp. 2–17, 2009.
[17] M. Xie, D. Wang, and L. Xie, "One SVR modeling method based on kernel space feature," *IEEJ Trans. Electr. Electron. Eng.*, vol. 13, no. 1, pp. 168–174, Jan. 2018.
[18] M. S. Ahmad, S. M. Adnan, S. Zaidi, and P. Bhargava, "A novel support vector regression (SVR) model for the prediction of splice strength of the unconfined beam specimens," *Construct. Building Mater.*, vol. 248, Jul. 2020, Art. no. 118475.
[19] K. Akatsu, K. Narita, Y. Sakashita, and T. Yamada, "Characteristics comparison between SPMSM and IPMSM under high flux density condition by both experimental and analysis results," in *Proc. Int. Conf. Elect. Mach. Syst.*, 2008, pp. 2848–2853.
[20] F. Wilcoxon, "Individual comparisons by ranking methods," *Biometrics Bull.*, vol. 1, no. 6, p. 80, Dec. 1945.

MINGHUA XIE was born in China in 1981. He received the B.S. degree in electronic and information engineering and the M.S. degree in circuits and systems from Northwest University in 2003 and 2006, respectively. He is currently pursuing the Ph.D. degree with the School of Automatic, Northwestern Polytechnical University. He is currently a Teacher with the School of Electronic Information and Electrical Engineering, Changsha University.

LILI XIE (Member, IEEE) was born in Shaanxi, China, in 1963. He received the M.Eng. and Ph.D. degrees in control theory and control engineering from Northwestern Polytechnical University, Xi'an, China, in 1989 and 1991, respectively.

He was with the Institute of Unmanned Aircraft from 1991 to 1996, where he became a Senior Engineer in 1996. He joined the Automation College, Northwestern Polytechnical University, where he was promoted to an Associate Professor in 1997 and a Full Professor in power electronics and drives in 2003. Since 1997, he has been engaged in teaching and research of electrical engineering and automation. His research interests include power electronics converters, electrical drives and control, power quality control, electrical fault diagnosis, and redundant control technology.